



Air ventilation assessment under unstable atmospheric stratification — A comparative study for Hong Kong

Weiwen Wang^{a,*}, Edward Ng^{a,b,c}

^a School of Architecture, The Chinese University of Hong Kong, Hong Kong SAR, China

^b Institute of Future Cities, The Chinese University of Hong Kong, Hong Kong SAR, China

^c Institute of Environment, Energy and Sustainability, The Chinese University of Hong Kong, Hong Kong SAR, China



ARTICLE INFO

Keywords:

Air ventilation assessment
Atmospheric boundary condition
Large-eddy simulation
Hong Kong

ABSTRACT

In most current air ventilation assessment (AVA) studies, a simple neutral assumption that does not consider thermal effects is adopted, particularly for numerical simulation practices. With statistics of daytime observations during summer in Hong Kong as an example, this study demonstrates that neutral atmospheric boundary conditions occur with a very low probability, which implies that current practices are indeed far away from reality. This study is devoted to addressing this knowledge gap by cross-comparisons of field measurements, wind tunnel tests, and large-eddy simulations (LES) under neutral and unstable conditions. It is found that LES-computed velocity ratios under unstable conditions are in line with field measurements, while results of simulations under neutral conditions are close to those of wind tunnel tests. Enhanced vertical mixing due to surface heating produces improved ventilation performance in the unstable case. The neutral assumption tends to underestimate pedestrian-level velocity ratios compared to a diabatic condition; hence it is deemed conservative when it is adopted in AVA practices. Moreover, stronger wind direction variance under unstable conditions results in weaker correlation between velocity ratios and frontal area indices than neutral conditions, which implies that street orientations become less important in ventilation under unstable conditions.

1. Introduction

Wind comfort and wind safety for pedestrians are important requirements for city design and urban planning [1]. For subtropical high-density cities such as Hong Kong, in order to mitigate the negative effects of the urban heat island, good ventilation is required for healthy living and comfortable thermal sensations [2,3]. After Hong Kong was hit by the Severe Acute Respiratory Syndrome (SARS), from which many people died in 2003, the Hong Kong government started discussions among various government departments and consulted relevant professional institutes and stakeholders regarding the standards, scope, and mechanism for application of an air ventilation assessment (AVA) system to improve the urban wind environment [4].

Afterwards, a set of planning guidelines was promoted based on a series of studies. The Housing, Planning and Lands Bureau and the Environment, Transport and Works Bureau jointly issued the Air Ventilation Assessment Technical Guidelines (AVA-TC06-01) in 2006. Meanwhile, a new chapter on ventilation assessment was also incorporated into the Hong Kong Planning Standards and Guidelines (HKPSG). These two documents, setting out the framework and

requiring all major government departments to include AVA as one of their planning and design considerations, were the first to address weak wind problems [5]. Unlike the guidelines of many countries for dealing with wind gust problems, the Hong Kong AVA is specifically designed to deal with weak wind conditions in congested urban areas under a hot and humid subtropical climate [4]. The world's first weak-wind urban AVA system has been applied in Hong Kong in the city's design and planning practices for more than a decade.

However, the current AVA methodology is known to have limitations in that it cannot correctly predict urban air ventilation performance in some areas of Hong Kong where convective motion is prominent due to inhomogeneous surface heating in weak wind conditions [6]. One possible cause is that the current AVA methodology adopts the neutral assumption for the atmospheric boundary condition, which is justified only when mechanical turbulence has a greater influence on ventilation than buoyancy-induced turbulence under high background wind speed. However, the neutral assumption does not adequately represent the actual situation, as the daytime atmospheric boundary is likely to be unstably stratified, particularly under clear sky and low wind conditions [7]. More importantly, the most crucial situations for

* Corresponding author. School of Architecture, The Chinese University of Hong Kong, Shatin, N.T., Hong Kong SAR, China.
E-mail address: w.wang@cuhk.edu.hk (W. Wang).

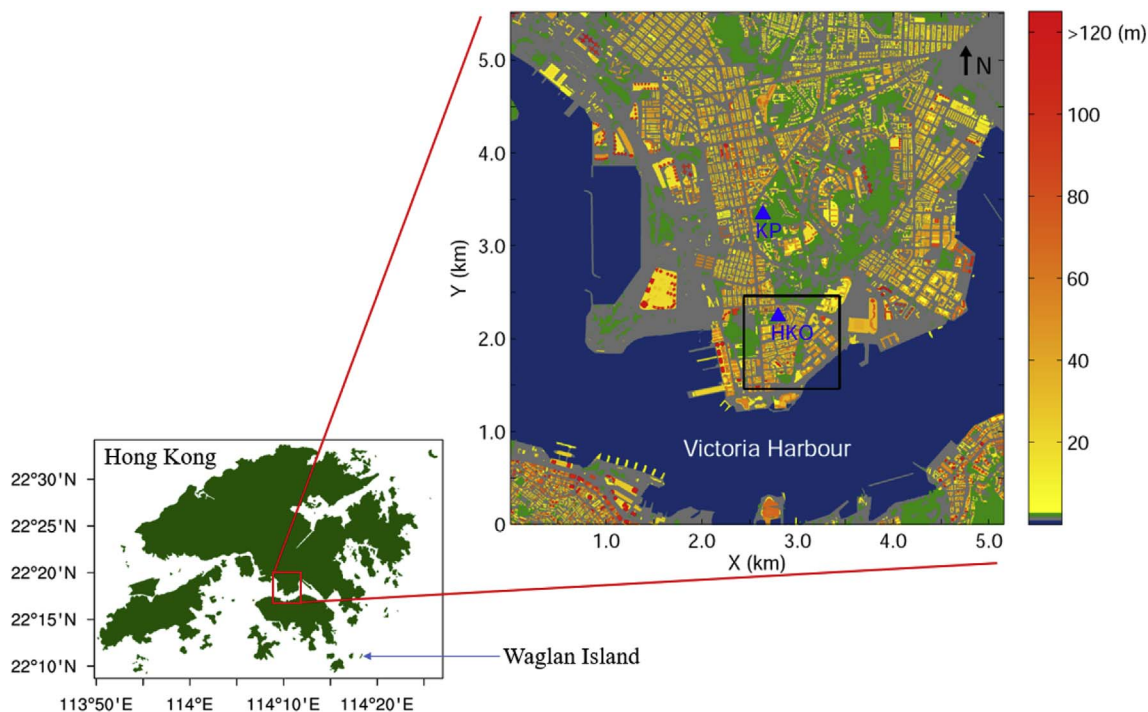


Fig. 1. High-density living environment in Hong Kong: urban morphology of the Kowloon Peninsula. The blue triangles denote the locations of two meteorological stations, Hong Kong Observatory Headquarters (HKO) and King's Park (KP). The black box encloses the domain of Tsim Sha Tsui. The colored bar describes building height (m). The location of Waglan Island is indicated. (For interpretation of the references to color in this figure legend, the reader is referred to the Web version of this article.)

urban ventilation are those in which only a low-speed background wind is present. The neutral assumption that supposes that buoyancy-induced turbulence has only a minor influence on ventilation is not true in such a condition.

The atmospheric stability of the urban boundary layer is well known [8]. Meanwhile, many urban ventilation studies have used wind tunnel testing and computational fluid dynamics (CFD) models with a neutral assumption [9–15]. But very few studies have addressed the effects of diabatic conditions on urban ventilation. A study of thermal effects on turbulence coherent structures found that when thermal effects are included by surface heating in large-eddy simulation (LES), the spanwise flow is stronger within an idealized building array compared to the neutral case [16]. Another LES study suggested that roof heating, in combination with building walls and ground heating, is important in the strength and location of the canyon vortex [17]. Both of these LES studies used idealized urban geometries (cubical building arrays). Using Reynolds-averaged Navier-Stokes (RANS) simulations of two simplified Hong Kong city models, Yang and Li pointed out that airflow in street canyons is dependent on thermal stratification when wind speed is small relative to the buoyancy force [18]. However, how pedestrian-level ventilation under thermal stratification differs from neutral conditions in a realistic urban complex is indistinct.

The neutral assumption is widely adopted in AVA practices, mainly because of its low computational cost and the ease with which it can be realized in numerical simulations and wind tunnel tests. When thermal conditions, specifically unstable stratification, are considered in ventilation, there will be additional challenges: First, a larger model domain is required to catch the larger turbulent structures in unstable simulations than in the neutral condition, while the grid size has to be kept small to sufficiently resolve the street-level air flows [19]. Second, special attention should be paid to the lateral boundary conditions to ensure that they will not artificially modify the wind environment within the assessment region. For instance, the radiative outflow condition in the non-cyclic boundary requires a positive outflow at all times [20,21]. Therefore, while a weak background wind is provided for generating buoyancy-driven turbulence, extra model domain is

needed on the leeward side of the city. This also requires extra computational cost. Third, more uncertainties will be incorporated in the estimation of initial thermal conditions. Heat fluxes are more difficult to monitor than winds. In such cases, validation of model results can be another obstacle.

The objective of this study is to demonstrate the knowledge gap between current practices and reality by comparing wind tunnel test results, field measurements, and a pair of LES experiments in Hong Kong, and to propose possible adaptations for future AVA practices based on the comparative results and knowledge of atmospheric boundaries under various conditions.

2. Data and methodology

In AVA studies, we are especially interested in pedestrian-level wind velocity. The wind velocity ratio (VR) is used as an indicator, which is calculated by $VR = V_p/V_\infty$, where V_p is the wind velocity at the pedestrian level (2 m above the ground), and V_∞ is the wind velocity at the boundary layer not affected by ground roughness. Apart from the meteorological data used in estimating the atmospheric stability class, this study includes some wind tunnel test results and field measurements from previous AVA studies, and a pair of LES experiments are undertaken for cross-comparison.

2.1. Observation and stability classification

Utilizing observations from two urban weather stations in Hong Kong during 2006–2015, we estimate the probability of stability classes according to Pasquill's atmospheric stability classification scheme [22]. Hourly cloud cover data are taken from Hong Kong Observatory Headquarters, while wind speed and global solar radiation data are taken from King's Park. The locations of these two weather stations are indicated in Fig. 1. We consider daytime hours (6 a.m.–8 p.m.) during all summer (June–August) days in 2006–2015.

As listed in Table 1, atmospheric turbulences are categorized into six stability classes, namely A, B, C, D, E, and F, with class A being the

Table 1
Pasquill stability classification scheme.

Surface Wind Speed at 10 m (ms^{-1})	Daytime Insolation			Nighttime Cloud Cover	
	Strong	Moderate	Slight	Thinly Overcast or $\geq 4/8$ Low Cloud	$\leq 3/8$ Cloud
< 2	A	A–B	B	–	–
2–3	A–B	B	C	E	F
3–5	B	B–C	C	D	E
5–6	C	C–D	D	D	D
> 6	C	D	D	D	D

most unstable, class F the most stable, and class D corresponding to neutral conditions. Thresholds for wind speed and cloud cover are quantitatively specified, while the threshold for daytime insolation is given only qualitatively, in terms of “strong,” “moderate,” and “slight,” which has to be transferred as specific values. Based on hourly observations of global solar radiation from 6 a.m. to 8 p.m. on summer days, the 25th, 50th, and 75th percentiles are computed as 0.16, 0.79, and 1.84 MJ m^{-2} , respectively. According to Table 1, daytime stability is classified. For example, when wind speed is lower than 2, classifications A and B are divided by the 50th percentile of solar radiation; when wind speed is between 2 and 3, classifications B and C are divided by the 75th percentile of solar radiation, classifications B and C are divided by the 25th percentile, and so forth.

The probability of various classes of stability is calculated using all summer data during 2006–2015. The estimated result suggests that neutral conditions occur with a very low probability of about only 2%; even the weak unstable class C occurs less than 20% of the time. During most of the daytime (about 80%), atmospheric stratification in urban Hong Kong can be classified as moderate and strongly unstable (classes B and A). However, the estimation may not be very accurate due to some deficiencies of this methodology. There are three limitations to the use of the Pasquill stability classification scheme: First, the Pasquill scheme is widely used mainly because it requires only routine meteorological data, but it was originally developed in the United Kingdom at a location some miles from the coast, and should be restricted to the insolation values and climate conditions there. It has been found that various stability classification methods result in large

discrepancies [23]. Second is the restriction of local observations to Hong Kong. HKO is one of the two sites that have cloud cover observations (the other site is Hong Kong International Airport). It is located in a small park that is surrounded by a high-density urban area in Tsim Sha Tsui (Fig. 1), with an altitude of 32 m above mean sea level. KP is surrounded by a relatively larger green space on a small hill with an altitude of 65 m on the Kowloon Peninsula. The uncertainties introduced to the classification of stability by such environmental conditions are difficult to control. Finally, there is no information available as to how the parameters of strong, moderate, and slight should be chosen when the Pasquill scheme is used locally in Hong Kong.

Due to the abovementioned limitations of stability classification using the Pasquill scheme and ordinary meteorological observations, we use some samples of radiosonde observations to further demonstrate the probability of various types of atmospheric conditions in Hong Kong in summer. The radiosonde data are observed at King’s Park (Fig. 1) and are available with open access from the University of Wyoming [24]. In practice, equivalent potential temperature (θ_e) is a useful measure of atmospheric stability. When θ_e increases with height, that is, $\frac{d\theta_e}{dz} > 0$, vertical motion is suppressed, and the atmospheric boundary is stably stratified. Correspondingly, $\frac{d\theta_e}{dz} < 0$ stands for an unstable boundary layer, and $\frac{d\theta_e}{dz} = 0$ represents a neutrally stratified atmospheric boundary layer.

Generally, sounding data are available only at 00:00 and 12:00 Greenwich Mean Time (GMT), that is, 08:00 and 20:00 Hong Kong local time. In this study, sounding data recorded at 20:00 local time are used. We demonstrate the results from September 2006 (Fig. 2), when the street-level field measurements (introduced in Section 2.3) are conducted. Meanwhile, data from July 2006, representing midsummer of the same year, are shown in Fig. 2 as well. Fig. 2a and b are the $\Delta\theta_e$ of the first recording level above 200 m (approximately above the street canyons) and the ground level (66 m, 1 m above the elevation of King’s Park) for July and September, respectively. Corresponding ΔZ is shown in Fig. 2c and d as a reference.

The sample result in July 2006 (Fig. 2a with two missing values) suggests that about 55.2% of the days are unstable ($\frac{d\theta_e}{dz} < 0$), about 31.0% are stable ($\frac{d\theta_e}{dz} > 0$), and about 13.8% are neutral ($\frac{d\theta_e}{dz} = 0$). Note that this was at 8 p.m., after sunset. The probability of unstable

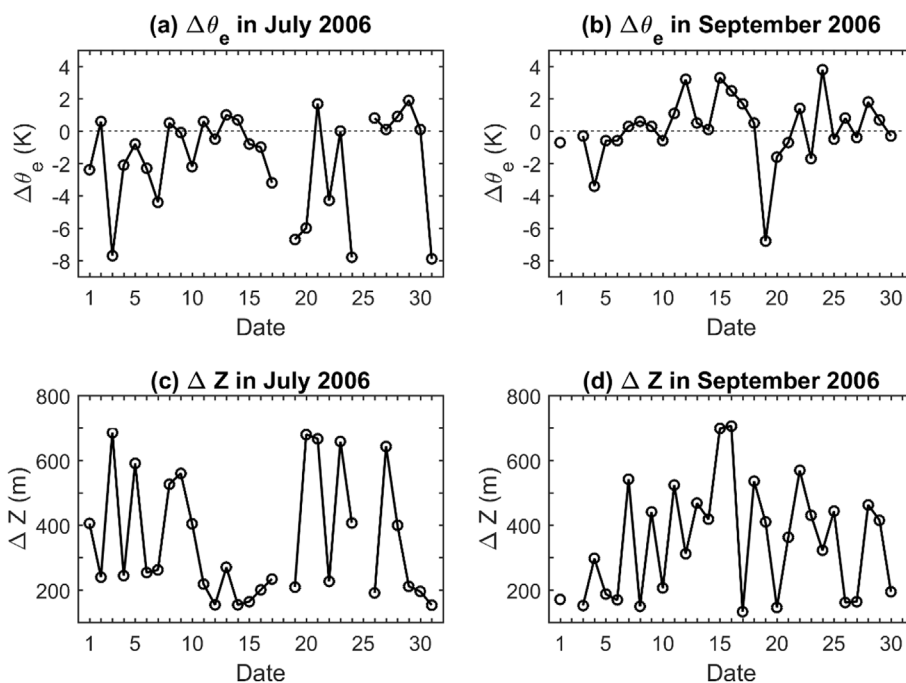


Fig. 2. Equivalent potential temperature difference ($\Delta\theta_e$) between the first recording level above 200 m and the ground level (66 m) taken from sounding measurements at King’s Park in (a) July and (b) September of 2006. The lower panel (c and d) demonstrates the corresponding height difference (ΔZ) of the two recording levels for July and September, respectively.

boundary conditions should increase during summer afternoon hours compared to this time. In September, when the weather is cooler, the probability of unstable conditions decreases while the probability of stable and near-neutral conditions increases compared to July (Fig. 2b).

In general, using both the Pasquill stability classification scheme and the vertical gradient of θ_e from radiosonde observations suggests that the probability of a neutrally stratified boundary layer in urban Hong Kong in summertime is not high; specifically, it is lower than the possibility of a thermally stratified boundary layer. The assumption of a neutral atmospheric boundary condition in air ventilation studies of Hong Kong is not representative.

2.2. Wind tunnel tests

Wind tunnel data are taken from an earlier AVA study [25]. The study was conducted by local researchers under the instruction of the Hong Kong Planning Department (HKPD). Final reports can be downloaded from the HKPD web page [26]. The wind tunnel tests were undertaken in accordance with international practice requirements and conducted at the CLP Power Wind/Wave Tunnel Facility (WWTF) of the Hong Kong University of Science and Technology [27]. The CLP Power WWTF has a state-of-the-art subsonic boundary-layer wind tunnel. The overall size is 61.5 m long \times 16.5 m wide \times 7.5 m high. Miniature hot-film anemometers are used for wind velocity measurements.

The wind tunnel model at Tsim Sha Tsui at the southern edge of the Kowloon Peninsula (Fig. 1) was chosen for the comparison. A 1:400 scale model of the study area and surrounding areas was fabricated to represent the state of the urban areas corresponding to the existing conditions in summer 2006. Wind velocities were measured at 5 mm from the ground, which corresponds to 2 m in reality. The top of the boundary layer was at a scale height of 500 m. Locations of all 94 test points at this wind tunnel site are shown in Fig. 3. Green dots denote test point group A (TSA, 31 points), blue dots denote test point group B (TSB, 29 points), and red dots denote test point group C (TSC, 34 points).

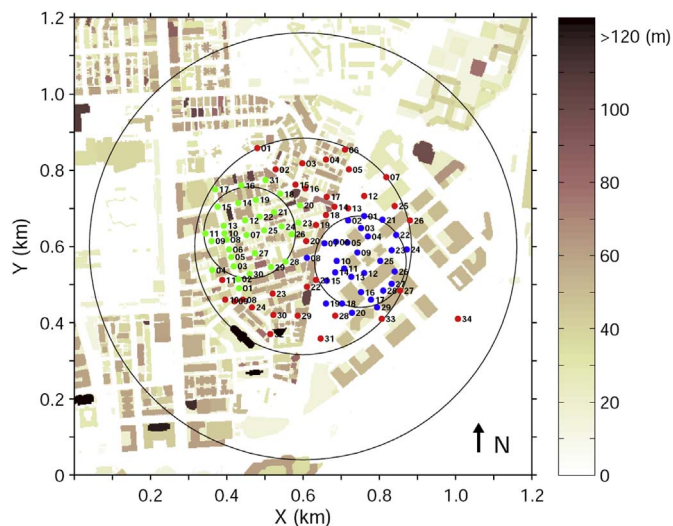


Fig. 3. Locations of test points in the wind tunnel model at Tsim Sha Tsui for comparison with field measurements and numerical simulations. Green dots denote test point group A (TSA), blue dots denote test point group B (TSB), and red dots denote test point group C (TSC). The largest circle is used to define this site in the wind tunnel test, and the middle and two small circles are used as a location reference for the grouped test points. The colored bar describes building heights (m) on the site. The wind comes from the east (right). (For interpretation of the references to color in this figure legend, the reader is referred to the Web version of this article.)

2.3. Field measurements

Ground measurement data are adopted from the field measurements in “Urban Climatic Map and Standards for Wind Environment – Feasibility Study” [28]. Spot measurements were conducted using handheld equipment along preselected paths in Tsim Sha Tsui. Measurements were made along the paths at fixed points (Fig. 4). The equipment used in the measurement included a 3-function sensor probe from TESTO [29] for the measurement of air temperature and wind speed, and a TESTO 400 data logger for instant processing of the measured data. The data logger was set with a sampling time of 10 s and an averaging time of 3 min. All the equipment was ISO certified and was cross-calibrated in the laboratory before actual measurements were taken.

Field measurements carried out on 19 September 2006 from 14:30 to 15:50 local time are utilized. It was a sunny and hot summer day. The air temperature observed at HKO during the field measurements was 28–29 °C, and the relative humidity was 60%–65%. The field measurements covered 54 measurement points and 1 reference point at the seafar in Tsim Sha Tsui (Fig. 4). Twelve trained researchers were employed and grouped into 6 teams to conduct the measurements. Each group started the measurements at the first point (close to the seashore) of their corresponding path at the same time; that is, Group 1 started at G1-1, while Group 2 started at G2-1, etc. (Fig. 4). During the measurements, measuring sensors were located 2 m above the ground and logged the data. When the measurement time was up, the researchers recorded the data and moved on to the next point at the designated time. Both temperature and wind speed were measured, but only wind data are used in this study. The values are listed in Table 2. The right-most column of Table 2 gives the time of measurement.

Mapping of the spatial distribution requires relatively stable weather conditions during the entire measurement period; that is, temporal variation of the weather conditions should be insignificant [30]. This requirement has been fulfilled for the field measurements used in this study. However, as all test points cannot be measured at the same time, uncertainties that could affect the results of the comparison between the measurements and numerical simulations are unavoidable. Moreover, the limited sampling time (5 min) for each point could import another uncertainty, as the LES represents a more stable situation with an hourly average. The realistic environment is difficult to fully consider in numerical modeling—for instance, the effects of greenery and traffic.

2.4. Large-eddy simulations

We employ an LES model to carry out CFD simulations in this study. LES overcomes the deficiencies of the RANS model by explicitly resolving large, energy-containing turbulent eddies and parameterizing only subgrid-scale (SGS) turbulence [31,32]. LES provides not only mean flow fields but also instantaneous turbulences, which are especially important for human comfort at the pedestrian level in the urban canopy layer.

2.4.1. The parallelized large-eddy simulation model (PALM)

The LES model used in this study is the Parallelized LES Model (PALM), which was developed in 1997, when it was one of the first parallelized LES models for atmospheric research [33]. The LES model has six prognostic quantities by default: the velocity components u , v , w on a Cartesian grid, the potential temperature θ , specific humidity q_v or a passive scalar s , and the SGS turbulent kinetic energy e . The governing equations are based on the non-hydrostatic, filtered, incompressible Navier-Stokes equations with Boussinesq approximation and are filtered implicitly using the volume-balance approach of Schumann [34]. The governing equations of PALM are given in Maronga et al. [35].

The modified version [36,37] of the 1.5-order Deardorff scheme

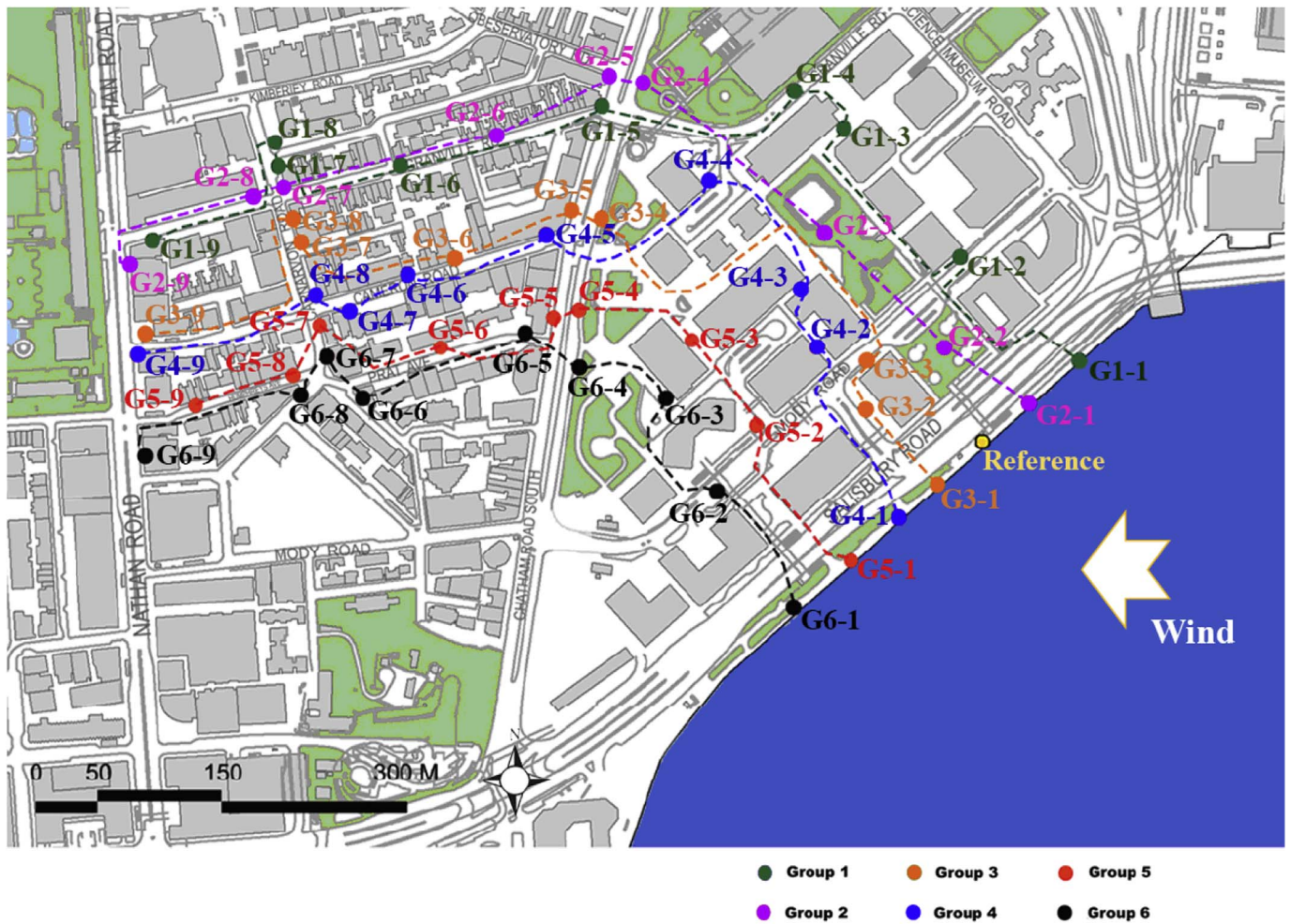


Fig. 4. Map of measurement paths and fixed measurement points in the Tsim Sha Tsui area.

Table 2
Measured wind speed (ms^{-1}) data at Tsim Sha Tsui on 19 September 2006.

	Group 1	Group 2	Group 3	Group 4	Group 5	Group 6	Time
Point 1	2.3	2.0	3.6	2.5	2.3	3.4	14:30
Point 2	2.3	3.6	2.6	1.6	3.1	2.3	14:40
Point 3	3.0	2.5	1.6	2.3	0.5	1.8	14:50
Point 4	0.9	0.8	1.4	1.5	1.8	2.5	15:00
Point 5	1.5	1.6	1.5	1.4	2.2	3.8	15:10
Point 6	0.9	1.0	1.6	1.2	1.2	2.4	15:20
Point 7	1.7	1.2	0.8	1.8	1.3	1.2	15:30
Point 8	1.4	1.0	1.5	1.5	1.6	3.0	15:40
Point 9	1.5	0.7	1.2	0.5	0.7	0.8	15:50

[38] is used for turbulence closure. The Temperton algorithm [39] for the fast Fourier transform is used to solve the Poisson equation for the perturbation pressure. For the time integration, a third-order Runge-Kutta scheme [40] is used. The advection scheme used is the second-order scheme of Piacsek and Williams [41]. Alternatively, a fifth-order scheme developed by Wicker and Skamarock [42] can be utilized. The Monin-Obukhov similarity theory (MOST) is applied between the surface and the first grid level. Following the MOST, a constant flux layer is assumed as the boundary condition between the surface and the first grid level where scalars and horizontal velocities are defined [35]. A Prandtl layer is assumed at each surface.

If non-cyclic horizontal boundary conditions are used, PALM provides the possibility of generating time-dependent turbulent inflow by using a turbulence-recycling method, which follows the one described

by Lund et al. [43] with modifications introduced by Kataoka and Mizuno [44]. In front of the simulation domain, a recycling area is attached. The outflow boundary of this recycling area is the recycling plane, from where the turbulence signal $\varphi'(y, z, t)$ is recycled:

$$\varphi'(y, z, t) = \varphi(x_{\text{recycle}}, y, z, t) - \varphi_y(z, t), \quad (1)$$

where x_{recycle} is the distance from the inflow boundary to the recycling plane, $\varphi_y(z, t)$ is the line average of a prognostic variable $\varphi \in \{u, v, w, \theta, e\}$ along y at $x = x_{\text{recycle}}$. $\varphi'(y, z)$ that is added to the mean inflow profile after each time step. The recycling area length x_{recycle} should be much larger than the integral length scale of the respective turbulent flow to avoid the same turbulence structures being recycled repeatedly. Hence a precursor run, which can have a comparatively small domain horizontally for generating the initial turbulence field of the main run, is promoted [35].

2.4.2. Experiment setups and simulation outputs

The computational domain is depicted in Fig. 5. The urban area is taken from the black box in Fig. 1, which encloses an area of 1 km by 1 km on the southeastern edge of the Kowloon Peninsula. In front of the city, a turbulence recycling area is added to the domain, where the turbulence-recycling method is applied to create a turbulent inflow for the simulation. The size of the recycling area is 480 m by 1 km, and it is 520 m away from the city area. The 520 m × 1 km buffer zone between x_{recycle} and the city helps prevent the blocking effects of the buildings from reaching the recycling area, while the 1 km × 1 km buffer zone on the leeward side of the city helps ensure a positive outflow. As introduced, the radiative outflow condition in this non-cyclic boundary

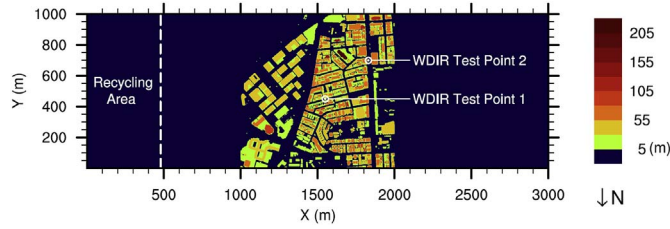


Fig. 5. The 3 km × 1 km LES model domain with the 1 km × 1 km urban topography (buildings) located in the middle. The white dashed line denotes $x_{recycle}$ in Eq. (1). The topography was rotated 180° (north is downward) to match the requirement of the turbulence-recycling method. The locations of the two test points for examining wind direction (WDIR) in Fig. 14 are indicated.

Table 3

Prescribed heat flux settings for 4 diabatic test runs and their output parameters of heat and velocity, and estimated bulk Richardson number (R_b).

Case	T_0	T_1	T_3	T_4
Rooftop heat flux (Kms^{-1})	0.005	0.1	0.2	0.3
Side wall heat flux (Kms^{-1})	0.005	0.01	0.02	0.03
θ_{CT} (K)	300.00	300.00	300.01	300.02
θ_0 (K)	300.05	300.08	300.13	300.16
U_{CT} (ms^{-1})	1.62	1.62	1.59	1.61
R_b	-0.12	-0.20	-0.31	-0.35

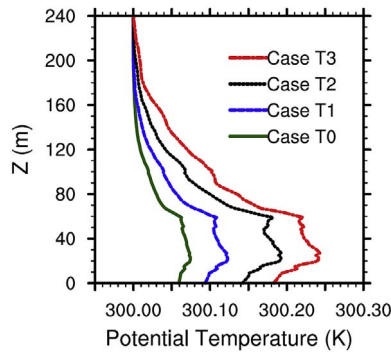


Fig. 6. Vertical profiles of potential temperature averaged from 3 y-z sections that cross the city ($x = 1400, 1500,$ and 1600 m in Fig. 5) in 4 diabatic LES test runs. The 4 runs are different in terms of prescribed heat fluxes to building rooftops and side walls. See Table 3 for details.

always requires a positive outflow. The topography was rotated 180° (north is downward) due to the requirement of the turbulence-recycling method that inflow must come from the left.

Horizontal grid spacing is equidistantly 2 m. Grid-sensitive tests using PALM 4.0 for urban ventilation simulations have been conducted in recent studies and suggest that a grid size of 2 m is sufficient for such a task [19,45]. Vertical grid spacing is 2 m below 300 m and is stretched with a stretch factor of 1.08 above. With 195 vertical levels, the top level is at about 1072 m. In the LES model, scalar variables are defined at the grid centers, while velocity components are shifted by half of the grid spacing. Therefore, horizontal wind velocity output from the 1 m and 3 m levels is linearly interpolated (averaged) to obtain V_p at 2 m above the ground. The no-slip bottom boundary condition and the free-slip top boundary condition are applied to the horizontal velocity components. A cyclic (periodic) boundary condition setup in the spanwise direction is implemented.

A low-velocity wind of 1.5 ms⁻¹ is prescribed. As introduced, we focus on the crucial situation for urban ventilation in which only a low-speed background wind is present. Under such low wind conditions, the influence of buoyancy-induced turbulence becomes important, and ventilation will depend on the balance between thermal forcing and wind forcing. In addition, if high wind speed is used, more

Table 4

Velocity ratio (VR) at 37 overlapping test points of wind tunnel and field measurements, and opposite values in LES experiments.

Wind tunnel test point ID	Field-measured point ID	Wind tunnel VR	Field-measured VR	LES neutral VR	LES unstable VR
TSC26	G1-3	0.25	0.47	0.24	0.39
TSC25	G1-4	0.09	0.14	0.08	0.17
TSC18	G1-5	0.28	0.23	0.19	0.36
TSA25	G1-6	0.13	0.14	0.05	0.12
TSA10	G1-7	0.12	0.27	0.04	0.20
TSA13	G1-8	0.17	0.22	0.12	0.19
TSB24	G2-3	0.21	0.39	0.30	0.43
TSC13	G2-4	0.19	0.13	0.28	0.33
TSC14	G2-5	0.20	0.25	0.15	0.27
TSA23	G2-6	0.20	0.16	0.07	0.22
TSA08	G2-7	0.15	0.19	0.06	0.17
TSA09	G2-8	0.21	0.16	0.11	0.16
TSB06	G3-4	0.23	0.22	0.21	0.37
TSB07	G3-5	0.25	0.23	0.15	0.19
TSA28	G3-6	0.08	0.25	0.15	0.29
TSA05	G3-7	0.09	0.13	0.12	0.18
TSA06	G3-8	0.19	0.23	0.11	0.25
TSC27	G4-2	0.20	0.25	0.12	0.32
TSB26	G4-3	0.28	0.36	0.31	0.22
TSB04	G4-4	0.12	0.23	0.10	0.20
TSB08	G4-5	0.34	0.22	0.28	0.19
TSA29	G4-6	0.25	0.19	0.21	0.14
TSA30	G4-7	0.24	0.28	0.12	0.31
TSA03	G4-8	0.05	0.23	0.02	0.33
TSC33	G5-2	0.29	0.48	0.21	0.50
TSB16	G5-3	0.12	0.08	0.05	0.08
TSB15	G5-4	0.32	0.28	0.40	0.31
TSC21	G5-5	0.24	0.34	0.11	0.39
TSC23	G5-6	0.19	0.19	0.11	0.23
TSA02	G5-7	0.09	0.20	0.14	0.16
TSC10	G5-8	0.20	0.25	0.17	0.24
TSB20	G6-3	0.09	0.28	0.06	0.30
TSB19	G6-4	0.47	0.39	0.41	0.59
TSC22	G6-5	0.44	0.59	0.38	0.59
TSC24	G6-6	0.11	0.38	0.06	0.32
TSA01	G6-7	0.12	0.19	0.16	0.24
TSC09	G6-8	0.32	0.47	0.31	0.43
Mean values		0.20	0.26	0.17	0.28
Standard deviations		0.10	0.11	0.10	0.12

computational time will be needed because the time step has to be shorter. But a low background wind speed also requires a large buffer zone behind the city to ensure a positive outflow (Fig. 5). The time step lengths are optimized in the LES model. In the LES experiments described below, the mean time step lengths are between 0.34 s (for the unstable cases) and 0.68 s (for the neutral case). A 1 h precursor run, with a horizontal domain of 240 m × 240 m and the same height as the main run, is promoted for generating initial turbulent inflow profiles. The total simulation time for the main run is 2 h. The first hour is excluded in the analysis of the results, as the turbulences need this time to spin-up. The simulated results of the second hour are averaged for analysis.

Simulations are performed with different atmospheric stratification. The first simulation features a neutral stratification in which the influence of temperature on the flow field is excluded; that is, the calculation of the temperature equation is switched off. In this case, the major output elements are velocity components. Other simulations feature an unstable stratification realized by a prescribed homogeneous potential temperature of 300 K below 800 m and a capping inversion layer above with a potential temperature gradient of 1 K per 100 m, which is a general temperature setup for simulations of a convective boundary layer. More importantly, prescribed heat fluxes are generated from building rooftops and side walls. As in a realistic urban area with rather complex urban form, the thermal conditions and their balance with the velocity field are difficult to quantitatively decide by heat flux

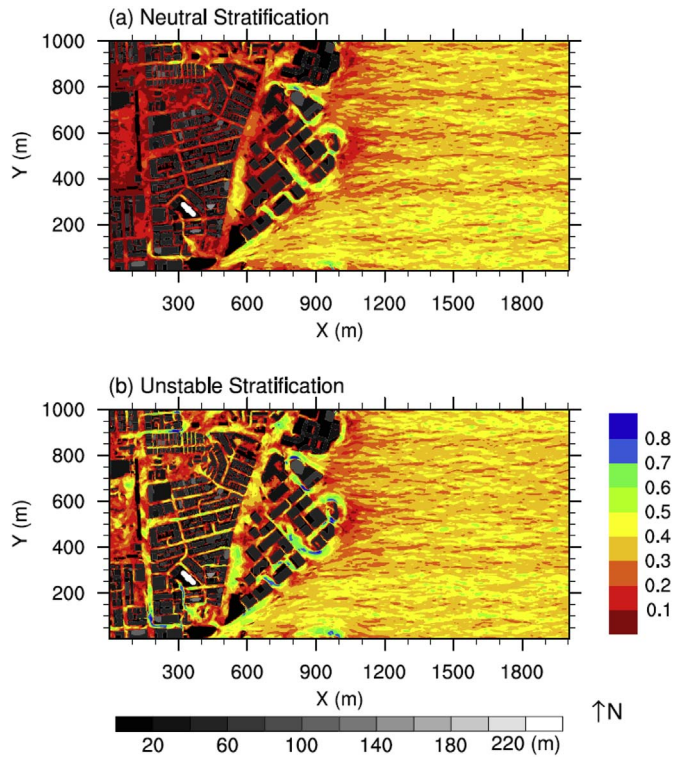


Fig. 7. LES-computed velocity ratio (VR) in Tsim Sha Tsui under (a) neutral conditions and (b) unstable conditions. Higher (lower) VR is described by cooler (hotter) colors in the vertical colored bar. The gray horizontal bar denotes building heights. The maps are rotated back to a normal orientation from the simulation, and the buffer zones behind the city are not shown. Input wind is from the east (right). (For interpretation of the references to color in this figure legend, the reader is referred to the Web version of this article.)

generation in the numerical simulation. Therefore, we carry out a set of test runs, namely T_0 , T_1 , T_2 , and T_3 , with various prescribed rooftop and side wall heat flux settings, as listed in Table 3. We deem that the approaching winds are always under neutral stratification due to general high wind speeds and very small surface roughness over open sea waters. Therefore, no surface heat fluxes are prescribed in the turbulence recycling area and the buffer zones.

The bulk Richardson number (R_b) is estimated to examine the unstable stratified boundary layers of the simulations:

$$R_b = gZ_{CT}(\theta_{CT} - \theta_0) / \{ \theta_0 (U_{CT})^2 \}, \quad (2)$$

where $g = 9.8 \text{ ms}^{-2}$ is the acceleration of gravity, Z_{CT} is the height of the canopy top, estimated at 200 m in this study (refer to Fig. 6), θ_0 is the potential temperature at the bottom (the lowest model level), and θ_{CT} and U_{CT} are the potential temperature and wind speed at the canopy top (200 m), respectively. The parameters in Table 3 are averaged from the

1 km \times 1 km city area. Herein, R_b for 4 diabatic test runs is estimated, ranging from -0.12 to -0.35 in Table 3. The more heat fluxes that are given in the LES, the larger the absolute R_b value that will be obtained. Fig. 6 demonstrates the potential temperature profiles averaged from 3 y-z sections that cross the city (at $x = 1400 \text{ m}$, 1500 m , and 1600 m in Fig. 5) from 4 diabatic LES experiments.

2.4.3. Model validation

The LES model has been validated for simulating flows and turbulence characteristics at the street-canyon and neighbourhood scale [46] and has been widely used in studies of urban street-canyon flows [47–50], including high-density urban areas in Hong Kong [51] and Macau [45]. The code used in this study (PALM version 4.0) has been validated by a CFD guideline [52] for pedestrian-level ventilation under neutral atmospheric conditions in recent studies [53,54]. For simulation of the thermally stratified urban boundary layer, the model has been validated by Uehara's wind tunnel data [55] for thermally stratified street canyons [56]. This study focuses on pedestrian-level ventilation. Simulation outputs from the LES model are cross-compared with wind tunnel tests (under neutral conditions) and field measurements (under unstable conditions), which will be presented in the following section.

3. Results

Wind tunnel test data, field measurements, and LES outputs are cross-compared to quantify their similarities and differences. We attempt to discover what causes deviations in pedestrian-level ventilation in different atmospheric conditions. In addition to wind speed, wind direction will be investigated as well. But first of all, we have to determine which diabatic simulation (T_0 , T_1 , T_2 , or T_3) best represents the typical actual boundary conditions.

3.1. Choice of diabatic simulation

The atmospheric stability of the urban boundary during the field measurements is estimated by meteorological observations. It is found that the hourly-averaged wind speed and global solar radiation observed at King's Park (Fig. 1) at 4 p.m. on 19 September 2006 are 2.9 ms^{-1} and 1.77 MJ m^{-2} , respectively. According to Pasquill's classification scheme (Table 1) and the thresholds introduced above (here we simply apply the summer thresholds to the field measurement days in September), it can be deduced that there were unstable (class B) atmospheric conditions at the time the field measurements were taken.

There are very few data regarding R_b in urban areas, and we are short of quantitative measurements for estimating R_b in the urban boundary in Hong Kong. Nakamura and Oke measured the temperature and wind distribution in a real street canyon and provided an R_b range from -0.45 to -0.17 on a clear midsummer afternoon [57]. The estimated values of R_b for the 4 diabatic runs in the present study, ranging from -0.12 to -0.35 (Table 3), are close to the field-measured values

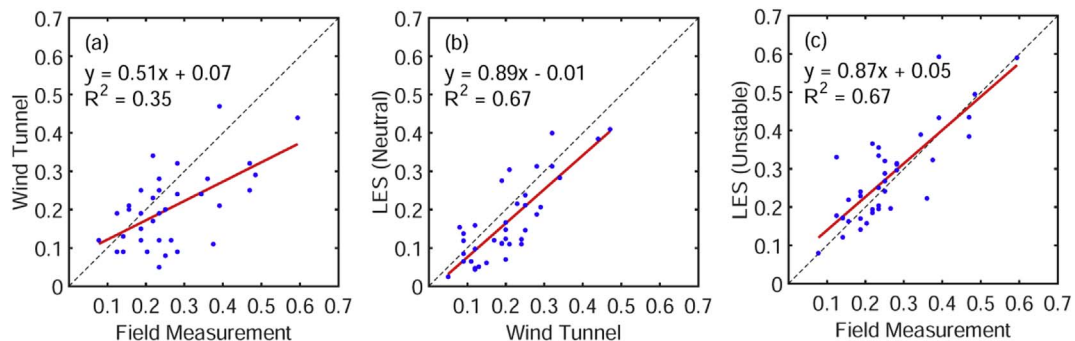


Fig. 8. Velocity ratio scatter plots and regressions of (a) field measurements and wind tunnel, (b) wind tunnel and neutral LES, and (c) field measurements and unstable LES.

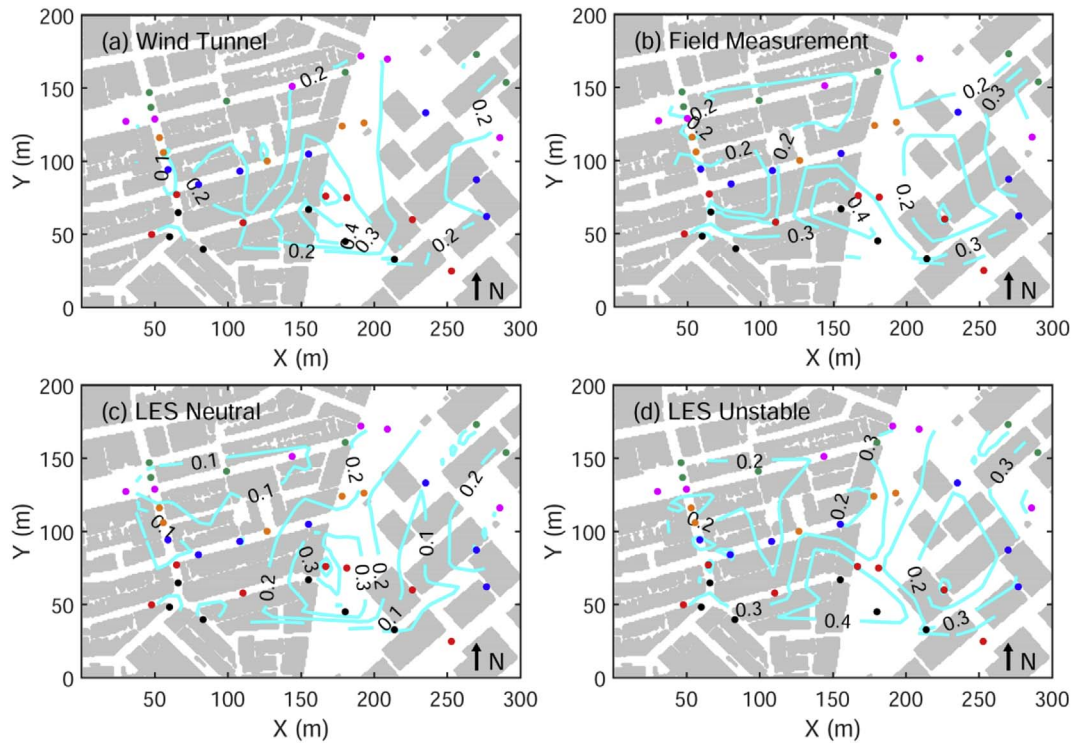


Fig. 9. Contour map velocity ratios meshed from the 37 test points of Table 4: (a) wind tunnel tests, (b) field measurements, (c) LES results of the neutral case, and (d) LES results of the unstable case. The overlapping test points of the wind tunnel tests and field measurements are demonstrated in colors, according to Fig. 4. (For interpretation of the references to color in this figure legend, the reader is referred to the Web version of this article.)

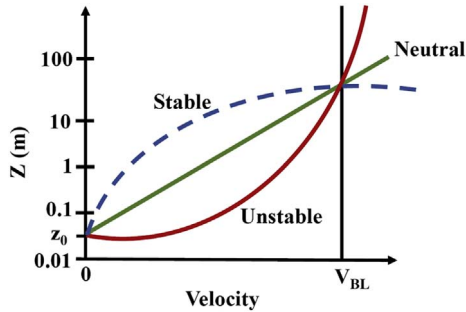


Fig. 10. Wind speed variation with height (Z) in the surface layer for different static stability classes plotted on a semi-log coordinate [60]. V_{BL} is the boundary-layer velocity.

of Nakamura and Oke [57]. The stratified conditions of the LES experiments can reproduce those observed in realistic urban areas.

Meanwhile, taking the comparison of the observed R_b in Nakamura and Oke [57] into consideration, wind tunnel experiments with thermal stratification by Uehara et al. [55] suggest a set of tested values of -0.12 , -0.19 , and -0.21 for a weakly to moderately unstable stratified urban boundary layer. Evaluating our LES results in Table 3 by this set of tested values in wind tunnel experiments of unstable stratification, T_1 , with an R_b of -0.2 , is deemed to be the best at reproducing a typical unstable stratified urban boundary layer. It is noteworthy that the wind tunnel speed V_∞ of Uehara et al. [55] is 1.5 ms^{-1} as well, the same as the setting in our LES experiments. Therefore, T_1 , with a mean kinematic heat flux of 0.1 Km^{-1} (about 117.5 W m^{-2}) prescribed to all building rooftops, and a mean kinematic heat flux of 0.01 Km^{-1} prescribed to all building side walls, is chosen as the final diabatic simulation for the following comparative study.

3.2. Cross-comparison of velocity ratios

It is difficult to estimate V_∞ in calculating VR for field

measurements. The reference point at the seafront (Fig. 4) is deemed unsuitable, as it measures near-surface (2 m above the ground) wind speed in front of the city. We propose the wind observed at Waglan Island as V_∞ . Waglan Island is located approximately 5 km southeast of Hong Kong Island and has uninterrupted exposure to winds (Fig. 1). With a very small surface roughness over open sea waters [58] and a relatively high anemometer elevation (83 m above mean sea level) [59], data collected at Waglan Island are considered to be representative of the boundary-layer wind approaching Hong Kong. Hourly wind speed observed at Waglan Island at 4 p.m. on 19 September 2006 is 6.4 ms^{-1} . The wind speeds in Table 2 are divided by this value to gain the field-measured VR.

Wind tunnel tests described in Section 2.2 are conducted under the neutral assumption. Among 94 wind tunnel test points and 55 field measurement points, there are 37 overlapping points (excluding the reference point at the seafront). The IDs of these 37 points in both the field measurements and wind tunnel tests are listed in Table 4, together with their corresponding VR values. The mean values in Table 4 suggest that the wind tunnel experiments may have underestimated the mean VR compared to field measurements.

LES-computed VR under neutral and unstable atmospheric conditions in Tsim Sha Tsui are shown in Fig. 7. It is obvious that the overall ventilation inside the city in the unstable experiment is better (with larger VR) than that in the neutral experiment. The overlapping test points of the wind tunnel and field measurements are located on the VR map of LES. Corresponding values are listed in Table 4 to enable cross-comparison. The mean values given in Table 4 show that the LES experiment under neutral conditions is more comparable to the wind tunnel tests, while the LES experiment under unstable conditions is more comparable to the field measurements. This is further demonstrated in the scatter plots and linear regressions in Fig. 8.

Fig. 8 shows that the wind tunnel predicts a relatively lower VR compared to field measurements, with a regression coefficient of 0.51 in Fig. 8a. Also, given an R-squared of 0.35, the regression between wind tunnel tests and field measurements is not very convincing. The

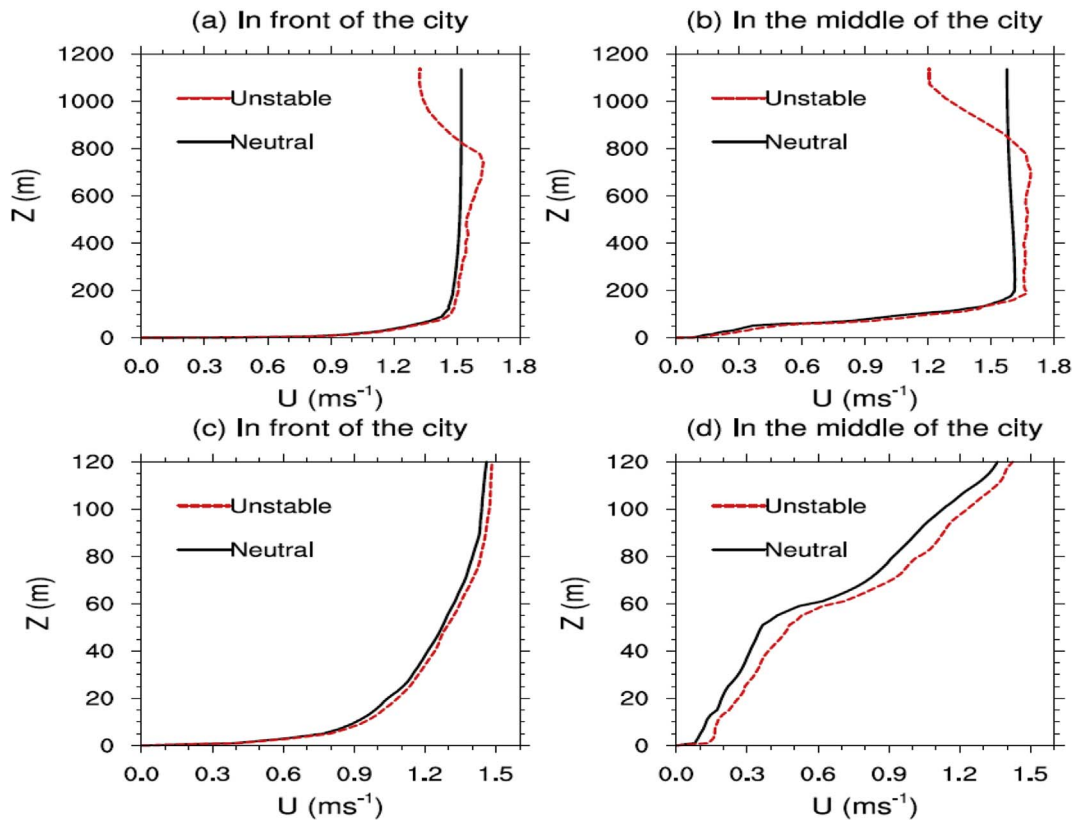


Fig. 11. LES-simulated zonal wind profiles: (a) in front of the city, (b) in the middle of the city, (c) in front of the city but below 120 m, and (d) in the middle of the city but below 120 m. Solid lines are the LES experiment under the neutral assumption, and dashed lines are under unstable stratification.

regression between the wind tunnel and LES neutral is better, with a regression coefficient closer to 1 (0.89) and a larger R-squared of 0.67 (Fig. 8b). The linear relation between field measurements and the diabatic LES experiment is like that of Fig. 8c, giving a regression coefficient of 0.87 and an R-squared of 0.67 (Fig. 8c). Moreover, geometrical features of pedestrian-level VR obtained from these methods are shown in Fig. 9. The best-ventilated areas are located around the main Chatham Road South (see Fig. 4) for all cases in Fig. 9. In the narrow streets west of Chatham Road South, VR is around 0.2 for field measurements and the LES unstable run, but decreases to about 0.1 in the LES neutral run and even below 0.1 in some areas in the wind tunnel tests.

3.3. Wind profile and thermal convection

According to our knowledge of boundary-layer meteorology, near-surface velocity over boundary-layer velocity is larger in an unstable atmospheric boundary layer than in a neutral one (Fig. 10). Therefore, the wind tunnel tests predict a lower VR for the 37 overlapping test points compared to the field measurements, which should be caused by the difference in atmospheric conditions; that is, neutral in the wind tunnel but unstable in the field measurements.

Wind profiles under different types of atmospheric boundary layers in Fig. 10 also explain why ventilation in the diabatic LES experiment is overall better than that under neutral conditions. Fig. 11 depicts some LES-simulated zonal wind (u -wind) profiles, both in front of the city and in the middle of the city. These profiles demonstrate that the diabatic LES experiment produces greater near-surface velocity than the neutral case, especially inside the city where surface (building) heating is provided.

The higher wind speed in the diabatic case is related to the additional convective motion caused by heating from the buildings, which increases vertical mixing throughout the boundary layer in and above

the city and leads to higher pedestrian-level ventilation compared to the neutral case. The vertical velocity sections in Fig. 12 show that in front of the city, the vertical velocity fluxes are generated by the turbulence recycling method, without the surface heating difference, and the diabatic case (Fig. 12b) is similar to the neutral case (Fig. 12a) in the lower levels. The differences in the top levels are produced by temperature gradients in the capping inversion. In the middle of the city, much stronger vertical motion is found in and above the street canyons in the unstable case (Fig. 12d) than in the neutral case (Fig. 12c).

3.4. Quantitative differences in simulations

The previous section illustrates that better ventilation under unstable conditions is caused by surface heating and enhanced vertical mixing. In this section, the differences between the LES experiments under neutral and unstable conditions will be quantitatively compared. This is shown in Fig. 13, which compares VRs taken from random test points in the city of the two LES experiments.

In this procedure, all street (unbuilt) grid points in each LES experiment are stored in a one-dimensional array, and 50,000 test points (about 30% of the total unbuilt grid points) are randomly taken from each array. The random function calculates the interval between test points using a normal distribution with a mean of the array size divided by the number of test points (50,000) and a standard deviation of 25% of the mean. The test points are randomly spread throughout the entire assessment area. Sensitivity tests were conducted regarding the number of test points, and no significant differences were found when the number of test points was larger than 50,000, which means that 50,000 test points are sufficient to produce the graphs in Fig. 13. Both the probability and the boxplot are produced by these 50,000 data points.

Fig. 13a shows that the diabatic LES experiment improves ventilation performance by increasing (decreasing) the probability of VR above (below) 0.15 compared to the neutral case. In each box of

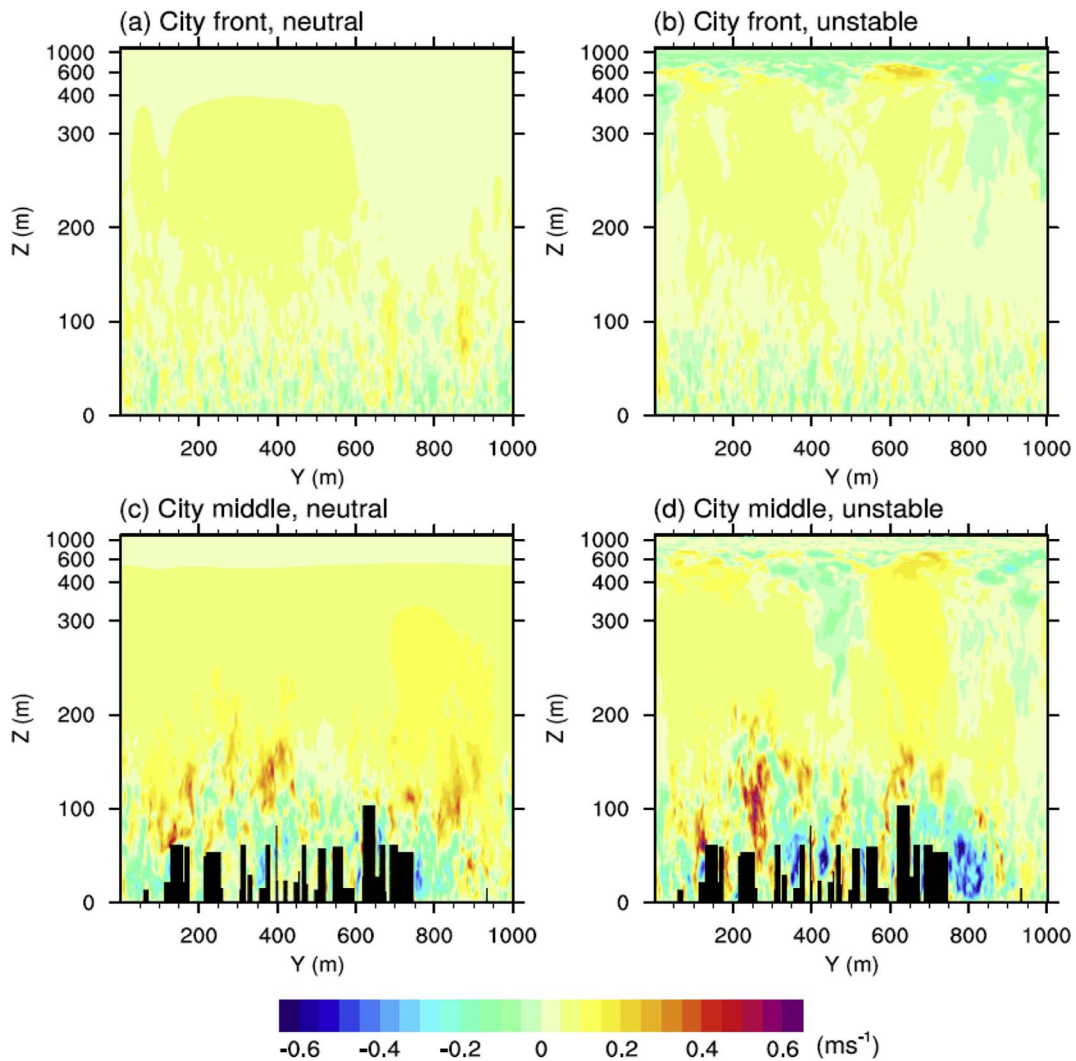


Fig. 12. Time-averaged vertical (y - z) sections of vertical velocity: (a) in front of the city under neutral conditions, (b) in front of the city under unstable conditions, (c) in the middle of the city under neutral conditions, and (d) in the middle of the city under unstable conditions. Warm colors represent rising motion, while cool colors denote sinking movement. (For interpretation of the references to color in this figure legend, the reader is referred to the Web version of this article.)

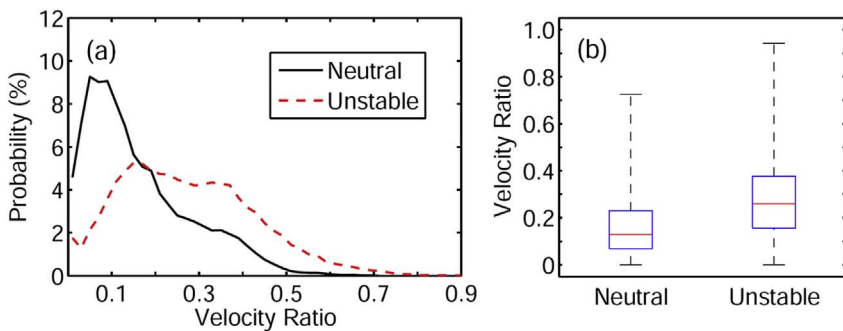


Fig. 13. Quantitative comparison of urban ventilation under neutral and unstable conditions in LES: (a) the probability of velocity ratios taken from random test points in the city of the two LES experiments, and (b) the boxplot of the two datasets. The outlier algorithm of the boxplot is ignored.

Fig. 13b, the central mark is the median, the edges of the box are the 25th and 75th percentiles, and the whiskers extend to the most extreme data points [61]. It is obvious that all statistics except the minimum value in the diabatic LES experiment are significantly larger than in the neutral case. The median of VR in the unstable case is 0.26, twice that in the neutral case (0.13). The maximum VR in the unstable and neutral cases is 0.94 and 0.73, respectively.

3.5. Impacts on wind direction variance

Additional convective motion caused by heating in the unstable experiment increases not only wind speed, but also fluctuations in wind direction. We select two points, one located in a narrow street parallel to the input wind direction (Point 1 as denoted in Fig. 5), the other located in a wide street perpendicular to the inflow wind direction (Point 2 as denoted in Fig. 5). The surrounding building shapes of these two points vary largely, but we focus only on the wind variation under the two atmospheric conditions, rather than the surrounding urban

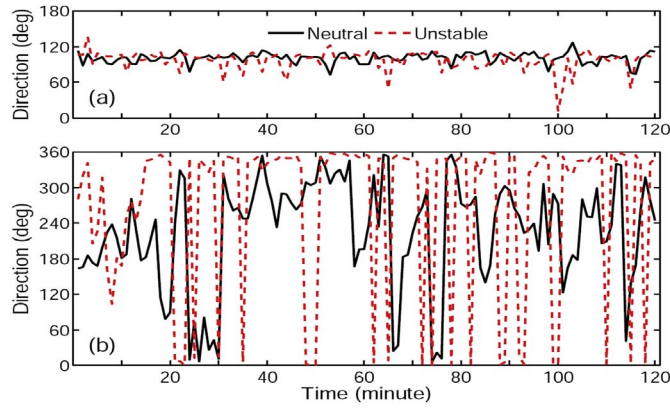


Fig. 14. Wind direction of (a) a grid point in a narrow parallel street, and (b) a grid point in a wide perpendicular street at 2 m above the ground. The solid line represents the neutral case and the dashed line represents the unstable case. The output interval is one minute.

forms. A time series of wind direction measured at 2 m above the ground during the last hour at these two grid points is shown in Fig. 14, with a solid line for the neutral case, a dashed line for the unstable case, and an output interval of 60 s.

Wind direction in the parallel street canyon is more homogeneous (Fig. 14a) compared to that in the perpendicular location (Fig. 14b), where intense rotations of wind occur in the lee of the buildings. But in both locations, we experience larger variance of wind direction in the unstable case than in the neutral case. Additional convective motion and enlarged eddy size due to surface heating should be major contributors to this difference in wind direction variance between the neutral and unstable cases.

Stronger variation in wind direction under unstable conditions implies that street orientation may be less important in urban ventilation compared to neutral conditions. This is verified by Fig. 15a. The frontal area index (λ_f), which is defined as the frontal area of buildings in a certain wind direction over a site area [62], is calculated from building data used in the simulations. This index has been widely used in urban wind environment investigations and is found to be an important morphological factor that influences urban ventilation [63,64]. We compute only the frontal area index, rather than frontal area density, as we have only one inflow wind direction. Frontal area density is the accumulation of frontal area indices in all wind directions, weighted by the observed occurrences of different directions.

Frontal area indices are calculated from $100\text{ m} \times 100\text{ m}$ averaging areas inside the $1\text{ km} \times 1\text{ km}$ city domain. In order to obtain more data samples, the averaging areas overlap. This is also a way to guarantee that the results are not influenced by random positioning of the averaging areas. In this procedure, the first averaging area covers a $100\text{ m} \times 100\text{ m}$ region in one corner, say, the left-bottom corner of the city domain. The next averaging area moves 20 m (10 model grids)

forward in one (x or y) direction, and so forth. In this way, a total of 2116 data samples are obtained in the 1 km^2 city domain. The VRs are also averaged in such a way in both the neutral and unstable cases.

Fig. 15a demonstrates that pedestrian-level VR under neutral conditions gives a correlation of -0.45 with the λ_f , which is significantly larger than -0.25 in the unstable case. Hence, street orientation seems to be less important for urban ventilation under unstable conditions due to larger wind direction variance compared to neutral conditions. The limitation of this is that the relationship between ventilation and λ_f is hard to justify given that only one wind angle is tested. Fig. 15b further demonstrates a scatter plot and regression between VR and the ground coverage ratio (λ_p), which is defined as the ratio of ground area that is covered by the building to the site area. This parameter is computed using the same averaging areas and moving-window algorithm that were used in the calculation of λ_f . More importantly, λ_p is independent of wind direction. Fig. 15 suggests that the correlation between VR and λ_p is higher than that between VR and λ_f in both the neutral and unstable cases. The VR under neutral conditions gives a correlation of -0.51 with λ_p , which is still larger than -0.4 in the unstable case (Fig. 15b). One possible cause is that stronger convective motion (Fig. 12) and greater wind direction variance (Fig. 14) in the unstable case reduce the effects of urban form and urban density on ventilation. Nevertheless, these results are still restricted by the limited domain and the complexity of the realistic urban morphology tested in the simulations. Future studies using parametric urban forms and urban densities while considering more input wind directions should be conducted to expand the preliminary result of this study.

4. Discussion

In general, the neutral assumption, which does not consider thermal stratification in air dynamics, is a simple but widely accepted assumption for urban wind studies. But the fact that neutral conditions occur with a relatively low probability in summertime, as shown in both the Pasquill stability classification scheme and the vertical gradient θ_e from radiosonde observations in Section 2.1, invokes the consideration of thermal stratification in studies of urban ventilation. In this case study, we cross-compare pedestrian-level VR taken from field measurements, wind tunnel tests, and a pair of LES experiments in a high-density area of Hong Kong.

The wind tunnel test under the neutral assumption is found to underestimate the ventilation as measured by pedestrian-level VR compared to the field measurements, which were taken during unstable atmospheric conditions (Fig. 8a). At the same time, the results of the LES experiment under the neutral assumption are consistent with those of the wind tunnel tests (Fig. 8b), while the unstable LES run captures the reality (field measurements) well (Fig. 8c). Such findings theoretically agree with our knowledge that near-surface wind speed over boundary-layer velocity should be significantly larger in unstable stratification than in neutral stratification (Fig. 10). The major cause is additional convective motion caused by surface heating, which

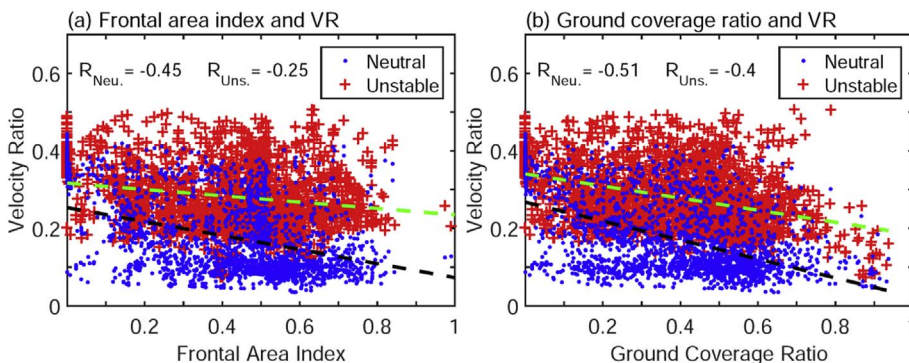


Fig. 15. Scatter plot of (a) velocity ratio and frontal area index λ_f , and (b) velocity ratio and ground coverage ratio λ_p . Blue dots denote the neutral LES experiment, and red crosses denote the unstable LES experiment. The black dashed line is the linear regression of the neutral case, and the green dashed line is the unstable case. (For interpretation of the references to color in this figure legend, the reader is referred to the Web version of this article.)

increases vertical mixing throughout the boundary layer in and above the city. These thermodynamical features are well captured by the LES experiments (Figs. 11 and 12). The quantitative difference in the LES results under neutral and unstable conditions are analyzed by VRs taken from random test points in the city (Fig. 13).

Impacts of different types of atmospheric conditions on wind direction variance in simulations of ventilation are evaluated. An unstable boundary induces stronger wind direction variance compared to a neutral boundary in the urban areas (Fig. 14). Therefore, the effects of street orientation on urban ventilation may be less important in an unstable boundary layer than in a neutral boundary layer. This is demonstrated by the regressions of the frontal area index and pedestrian-level VR under different types of atmospheric conditions (Fig. 15).

According to the findings in Sections 3.2–3.4, we can deduce that current AVA practices under the neutral assumption are conservative if the actual atmospheric boundary is unstably stratified. But it is also noteworthy that unstable stratification generally occurs under weak wind conditions (Table 1). As the background wind (the boundary-layer velocity in Fig. 10) is weak, though the pedestrian-level VR under unstable conditions is significantly larger than that under neutral conditions, the actual wind environment, that is, the absolute wind speed at the pedestrian level, will not improve as much as the VR.

We considered only neutral and unstable stratifications in this study and did not look at stable stratification. Urban ventilation studies under stable atmospheric conditions are difficult due to a lack of in situ observations, and modeling (with a wind tunnel or CFD) of this type of thermal stratification is challenging. But the effects of a stably stratified boundary on urban ventilation should be the subject of a future study. According to Fig. 10, stable boundary conditions may be the worst situation for urban ventilation, as they produce the smallest near-surface velocity over boundary-layer velocity compared to the other two types of conditions, and the background wind is generally not very strong (Table 1).

5. Conclusions

To conclude, wind tunnel tests under the neutral assumption underestimate the overall ventilation as measured by pedestrian-level VR compared to field measurements, which were conducted during an unstably stratified atmospheric boundary. VRs in the unstable LES case are in line with field measurements, while those in the neutral case are close to the wind tunnel tests. Overall ventilation under unstable conditions is found to be better than that under neutral conditions. Current AVA practices under the neutral assumption are conservative if the actual situation includes an unstably stratified boundary layer. Enhanced convective motion due to surface heating in unstable conditions is the main reason the neutral assumption can be conservative. Moreover, stronger wind direction variance under unstable conditions results in weaker correlation between VRs and frontal area indices than under neutral conditions. This implies that street orientation is less important in street-level ventilation under unstable conditions than in neutral conditions, due to the importance of surface heating effects in unstable conditions.

Acknowledgments

This study was supported by the Research Grants Council of the Hong Kong Special Administrative Region [grant number 14408214].

References

- [1] B. Blocken, W.D. Janssen, T. van Hooff, CFD simulation for pedestrian wind comfort and wind safety in urban areas: general decision framework and case study for the Eindhoven University campus, *Environ. Model. Software* 30 (2012) 15–34.
- [2] W. Wang, W. Zhou, E.Y.Y. Ng, Y. Xu, Urban heat islands in Hong Kong: statistical modeling and trend detection, *Nat. Hazards* 83 (2016) 885–907.
- [3] E. Ng, V. Cheng, Urban human thermal comfort in hot and humid Hong Kong,

- Energy Build.* 55 (2012) 51–65.
- [4] E. Ng, Policies and technical guidelines for urban planning of high-density cities – air ventilation assessment (AVA) of Hong Kong, *Build. Environ.* 44 (2009) 1478–1488.
- [5] R. Emmanuel, *Urban Climate Challenges in the Tropics: Rethinking Planning and Design Opportunities*, Imperial College Press, London, 2016.
- [6] E. Ng, J. Fung, Determining site wind availability for air ventilation assessment in Hong Kong's coastal and highly complex topographical conditions, in: C.K. Choi (Ed.), *The 4th International Conference on Advances in Wind & Structures (AWAS'08)*, Seoul, Korea, 2008, pp. 29–31.
- [7] W. Wang, E. Ng, S. Raasch, H.L. Yim, C.K. Ho, Parametric studies of urban morphologies of high density cities and their air ventilation performance under neutral and unstable atmospheric conditions using advanced large-eddy simulations, *The 9th International Conference on Urban Climate (ICUC)*, Toulouse, France, 2015, pp. 1–6.
- [8] J.F. Barlow, Progress in observing and modelling the urban boundary layer, *Urban Climate* 10 (2014) 216–240.
- [9] C. Yuan, E. Ng, Building porosity for better urban ventilation in high-density cities – a computational parametric study, *Build. Environ.* 50 (2016) 176–189.
- [10] J. Hang, Z. Luo, M. Sandberg, J. Gong, Natural ventilation assessment in typical open and semi-open urban environments under various wind directions, *Build. Environ.* 70 (2013) 318–333.
- [11] B. Blocken, T. Stathopoulos, J.P.A.J. van Beeck, Pedestrian-level wind conditions around buildings: review of wind-tunnel and CFD techniques and their accuracy for wind comfort assessment, *Build. Environ.* 100 (2016) 50–81.
- [12] F. Yang, Y. Gao, K. Zhong, Y. Kang, Impacts of cross-ventilation on the air quality in street canyons with different building arrangements, *Build. Environ.* 104 (2016) 1–12.
- [13] Q.M. Zahid Iqbal, A.L.S. Chan, Pedestrian level wind environment assessment around group of high-rise cross-shaped buildings: effect of building shape, separation and orientation, *Build. Environ.* 101 (2016) 45–63.
- [14] L. Chen, J. Hang, M. Sandberg, L. Claesson, S. Di Sabatino, H. Wigo, The impacts of building height variations and building packing densities on flow adjustment and city breathability in idealized urban models, *Build. Environ.* 118 (2017) 344–361.
- [15] Z.T. Ai, C.M. Mak, CFD simulation of flow in a long street canyon under a perpendicular wind direction: evaluation of three computational settings, *Build. Environ.* 114 (2017) 293–306.
- [16] S.-B. Park, J.-J. Baik, A large-eddy simulation study of thermal effects on turbulence coherent structures in and above a building array, *J. Appl. Meteorol. Climatol.* 52 (2013) 1348–1365.
- [17] N. Nazarian, J. Kleissl, Realistic solar heating in urban areas: air exchange and street-canyon ventilation, *Build. Environ.* 95 (2016) 75–93.
- [18] L. Yang, Y. Li, Thermal conditions and ventilation in an ideal city model of Hong Kong, *Energy Build.* 43 (2011) 1139–1148.
- [19] T. Gronemeier, S. Raasch, E. Ng, Effects of unstable stratification on ventilation in Hong Kong, *Atmosphere* 8 (2017) 168.
- [20] I. Orlanski, A simple boundary condition for unbounded hyperbolic flows, *J. Comput. Phys.* 21 (1976) 251–269.
- [21] M.J. Miller, A.J. Thorpe, Radiation conditions for the lateral boundaries of limited-area numerical models, *Q. J. Roy. Meteorol. Soc.* 107 (1981) 615–628.
- [22] F. Pasquill, The estimation of the dispersion of windborne material, *Meteorol. Mag.* 90 (1961) 33–49.
- [23] M. Mohan, T.A. Siddiqui, Analysis of various schemes for the estimation of atmospheric stability classification, *Atmos. Environ.* 32 (1998) 3775–3781.
- [24] University of Wyoming. <http://weather.uwyo.edu/upperair/sounding.html>. Last accessed on November 21, 2017.
- [25] Hong Kong Planning Department, Working Paper 2B: wind tunnel benchmarking studies, Urban climatic map and standards for wind environment - feasibility study, 2008, pp. 1–587.
- [26] HKPD. http://www.pland.gov.hk/pland_en/p_study/prog_s/ucmapweb/index.htm. Last accessed on February 9, 2017.
- [27] WWTF. <http://www.wwtf.ust.hk/facilities.html>. Last accessed on November 28, 2017.
- [28] Hong Kong Planning Department, Methodologies and results of field measurement, Urban Climatic Map and Standards for Wind Environment - Feasibility Study, 2008, pp. 1–73.
- [29] TESTO. <https://www.testo.com/en/>. Last accessed on November 23, 2017.
- [30] Y. Shi, C. Ren, Y. Zheng, E. Ng, Mapping the urban microclimatic spatial distribution in a sub-tropical high-density urban environment, *Architect. Sci. Rev.* 59 (2016) 370–384.
- [31] W. Rodi, J.H. Ferziger, M. Breuer, Pourquoiée M. Status of large eddy simulation: results of a workshop, *J. Fluid Eng.* 119 (1997) 248–262.
- [32] T. Tamura, Towards practical use of LES in wind engineering, *J. Wind Eng. Ind. Aerod.* 96 (2008) 1451–1471.
- [33] S. Raasch, M. Schröter, PALM - a large-eddy simulation model performing on massively parallel computers, *Meteorol. Z.* 10 (2001) 363–372.
- [34] U. Schumann, Subgrid scale model for finite difference simulations of turbulent flows in plane channels and annuli, *J. Comput. Phys.* 18 (1975) 376–404.
- [35] B. Maronga, M. Gryschka, R. Heinze, F. Hoffmann, F. Kanani-Sühring, M. Keck, et al., The Parallelized Large-Eddy Simulation Model (PALM) version 4.0 for atmospheric and oceanic flows: model formulation, recent developments, and future perspectives, *Geosci. Model Dev. Discuss. (GMDD)* 8 (2015) 1539–1637.
- [36] C.H. Moeng, J.C. Wyngaard, Spectral analysis of large-eddy simulations of the convective boundary layer, *J. Atmos. Sci.* 45 (1988) 3573–3587.
- [37] E.M. Saiki, C.H. Moeng, P.P. Sullivan, Large-eddy simulation of the stably stratified planetary boundary layer, *Boundary-Layer Meteorol.* 95 (2000) 1–30.

- [38] J.W. Deardorff, Stratocumulus-capped mixed layers derived from a three-dimensional model, *Boundary-Layer Meteorol.* 18 (1980) 495–527.
- [39] C. Temperton, A generalized prime factor FFT algorithm for any $N = 2^p 3^q 5^r$, *SIAM J. Sci. Stat. Comput.* (1992) 676–686.
- [40] J.H. Williamson, Low-storage Runge-Kutta schemes, *J. Comput. Phys.* 35 (1980) 48–56.
- [41] S.A. Piacsek, G.P. Williams, Conservation properties of convection difference schemes, *J. Comput. Phys.* 198 (1970) 580–616.
- [42] L.J. Wicker, W.C. Skamarock, Time-splitting methods for elastic models using forward time schemes, *Mon. Weather Rev.* 130 (2002) 2088–2097.
- [43] T.S. Lund, X. Wu, K.D. Squires, Generation of turbulent inflow data for spatially-developing boundary layer simulations, *J. Comput. Phys.* 140 (1998) 233–258.
- [44] H. Kataoka, M. Mizuno, Numerical flow computation around aeroelastic 3D square cylinder using inflow turbulence, *Wind Struct.* 5 (2002) 379–392.
- [45] M. Keck, S. Raasch, M.O. Letzel, E. Ng, First results of high resolution large-eddy simulations of the atmospheric boundary layer, *J. Heat Island. Int. Inst.* 9 (2014) 39–43.
- [46] M.O. Letzel, M. Krane, S. Raasch, High resolution urban large-eddy simulation studies from street canyon to neighbourhood scale, *Atmos. Environ.* 42 (2008) 8770–8784.
- [47] M. Kanda, A. Inagaki, T. Miyamoto, M. Gryschka, S. Raasch, A new aerodynamic parameterization for real urban surfaces, *Boundary-Layer Meteorol.* 148 (2013) 357–377.
- [48] A.A. Razak, A. Hagishima, N. Ikegaya, J. Tanimoto, Analysis of airflow over building arrays for assessment of urban wind environment, *Build. Environ.* 59 (2013) 56–65.
- [49] A. Inagaki, M.C.L. Castillo, Y. Yamashita, M. Kanda, H. Takimoto, Large-eddy simulation of coherent flow structures within a cubical canopy, *Boundary-Layer Meteorol.* 142 (2011) 207–222.
- [50] S.-B. Park, J.-J. Baik, Large-eddy simulations of convective boundary layers over flat and urbanlike surfaces, *J. Atmos. Sci.* 71 (2014) 1880–1892.
- [51] M.O. Letzel, C. Helmke, E. Ng, X. An, A. Lai, S. Raasch, LES case study on pedestrian level ventilation in two neighbourhoods in Hong Kong, *Meteorol. Z.* 21 (2012) 575–589.
- [52] Y. Tominaga, A. Mochida, R. Yoshie, H. Kataoka, T. Nozu, M. Yoshikawa, et al., AIJ guidelines for practical applications of CFD to pedestrian wind environment around buildings, *J. Wind Eng. Ind. Aerod.* 96 (2008) 1749–1761.
- [53] W. Wang, E. Ng, C. Yuan, S. Raasch, Large-eddy simulations of ventilation for thermal comfort — a parametric study of generic urban configurations with perpendicular approaching winds, *Urban Climate* 20 (2017) 202–227.
- [54] W. Wang, Y. Xu, E. Ng, S. Raasch, Evaluation of satellite-derived building height extraction by CFD simulations: a case study of neighborhood-scale ventilation in Hong Kong, *Landsc. Urban Plann.* 170 (2018) 90–102.
- [55] K. Uehara, S. Murakami, S. Oikawa, S. Wakamatsu, Wind tunnel experiments on how thermal stratification affects flow in and above urban street canyons, *Atmos. Environ.* 34 (2000) 1553–1562.
- [56] S.-B. Park, J.-J. Baik, S. Raasch, M.O. Letzel, A large-eddy simulation study of thermal effects on turbulent flow and dispersion in and above a street canyon, *J. Appl. Meteorol. Climatol.* 51 (2012) 829–841.
- [57] Y. Nakamura, T.R. Oke, Wind, temperature and stability condition in an East-West oriented urban canyon, *Atmos. Environ.* 22 (1988) 2691–2700.
- [58] S.A. Hsu, E.A. Meindl, D.B. Gilhousen, Determining the power-law wind-profile exponent under near-neutral stability conditions at sea, *J. Appl. Meteorol.* 33 (1994) 757–765.
- [59] L.W. Siu, M.A. Hart, Quantifying urban heat island intensity in Hong Kong SAR, China, *Environ. Monit. Assess.* 185 (2013) 4383–4398.
- [60] R.B. Stull, *An Introduction to Boundary Layer Meteorology*, Kluwer Academic Publishers, Dordrecht, Netherlands, 1988.
- [61] R. McGill, J.W. Tukey, W.A. Larsen, Variations of boxplots, *Am. Statistician* 32 (1978) 12–16.
- [62] Y. Xu, C. Ren, P. Ma, J. Ho, W. Wang, K.K.-L. Lau, et al., Urban morphology detection and computation for urban climate research, *Landsc. Urban Plann.* 167 (2017) 212–224.
- [63] E. Ng, C. Yuan, L. Chen, C. Ren, J.C.H. Fung, Improving the wind environment in high-density cities by understanding urban morphology and surface roughness: a study in Hong Kong, *Landsc. Urban Plann.* 101 (2011) 59–74.
- [64] M. Lin, J. Hang, Y. Li, Z. Luo, M. Sandberg, Quantitative ventilation assessments of idealized urban canopy layers with various urban layouts and the same building packing density, *Build. Environ.* 79 (2014) 152–167.